

## THE EMERGENCE OF A TWISTED MAGNETIC FLUX TUBE INTO A PREEXISTING CORONAL ARCADE

Y. FAN AND S. E. GIBSON

High Altitude Observatory, National Center for Atmospheric Research,<sup>1</sup> P.O. Box 3000, Boulder, CO 80307

Received 2003 March 14; accepted 2003 April 16; published 2003 April 29

### ABSTRACT

To investigate the dynamic evolution of a coronal magnetic field in response to the emergence of significantly twisted magnetic structures, we perform MHD simulations in the low- $\beta$  regime of the emergence of a twisted magnetic flux tube into a preexisting coronal potential magnetic arcade. Our simulation of a twisted flux tube, which when fully emerged contains a twist of  $1.875 \times 2\pi$  field-line rotation about the axis between the anchored footpoints, leads to a magnetic structure with substantial writhing of the tube axis (with an apex rotation  $>90^\circ$ ) as a result of the nonlinear evolution of the kink instability. For an emerging tube with a left-handed twist (which is the preferred sense of twist for active regions in the northern hemisphere), the writhing of the tube is also left-handed, producing a forward-S shape for the tube axis as viewed from the top, which is opposite to the inverse-S-shaped X-ray sigmoid structures preferentially seen in the northern hemisphere. However, we find that the writhing motion of the tube and its interaction with the ambient coronal magnetic field also drive the formation of an intense current layer that displays an inverse-S shape, consistent with the shape of X-ray sigmoids.

*Subject headings:* MHD — Sun: corona — Sun: magnetic fields

### 1. INTRODUCTION

Soft X-ray images of solar active regions frequently show S-shaped or inverse-S-shaped morphology called “X-ray sigmoids,” with the northern (southern) hemisphere preferentially showing an inverse-S (forward-S) shape (e.g., Rust & Kumar 1996; Pevtsov, Canfield, & Latushko 2001). Understanding the nature of these X-ray sigmoids is important since active regions showing X-ray sigmoid structures are found to be statistically more likely to produce flares and coronal mass ejections (Canfield, Hudson, & McKenzie 1999). One possibility is that these sigmoid structures form because of the direct emergence of twisted magnetic flux tubes from the interior into the corona. Several simulations of the emergence of twisted flux tubes have shown that one can readily find emerged field lines displaying both forward-S and inverse-S sigmoid morphology for an emerging tube of one sign of twist (e.g., Magara & Longcope 2001, 2003; Abbett & Fisher 2003). Since X-ray sigmoid brightenings most likely correspond to sites of enhanced magnetic energy dissipation and heating as a result of the formation of intense electric current layers (Titov & Demoulin 1999; Low & Berger 2003), it is important to study the three-dimensional structure of the electric current concentration in the corona resulting from the emergence of twisted flux tubes. In this Letter, we present a three-dimensional MHD simulation of the emergence of a twisted magnetic flux tube into a preexisting coronal potential magnetic arcade and study the three-dimensional structure of the electric current concentration that forms as the emerging tube develops substantial writhing as a result of the kink instability.

### 2. MODEL DESCRIPTION

Our focus is the evolution of the coronal magnetic field under the conditions of high electric conductivity and low-plasma  $\beta$

(the ratio of gas pressure over magnetic pressure). We solve the following MHD equations:

$$\frac{\partial \rho}{\partial t} + \nabla \cdot (\rho \mathbf{v}) = 0, \quad (1)$$

$$\rho \left[ \frac{\partial \mathbf{v}}{\partial t} + (\mathbf{v} \cdot \nabla) \mathbf{v} \right] = -\nabla p + \frac{1}{4\pi} (\nabla \times \mathbf{B}) \times \mathbf{B} + \rho \nu \nabla^2 \mathbf{v}, \quad (2)$$

$$\frac{\partial \mathbf{B}}{\partial t} = \nabla \times (\mathbf{v} \times \mathbf{B}), \quad (3)$$

$$\nabla \cdot \mathbf{B} = 0, \quad (4)$$

with an isothermal equation of state  $p = \rho a_s^2$ , drastically simplifying the treatment of the energy equation and the thermodynamics of the coronal plasma. We let the isothermal sound speed  $a_s$  be much smaller than the characteristic Alfvén speed  $v_A$  (with  $a_s$  set to  $0.022v_A$  and  $v_A$  defined below). In the momentum equation (eq. [2]), the Lorentz force dominates. Gravity is ignored, and the pressure gradient is negligible compared with the Lorentz force, except at the locations of intense current layers. There is also an explicit viscous term with a constant viscosity  $\nu$ , such that the ratio of the viscous timescale,  $\tau_\nu = L^2/\nu$ , over the dynamic timescale,  $\tau_A \equiv L/v_A$ , is  $\tau_\nu/\tau_A = Lv_A/\nu = 500$ , where  $L$  is the size scale of the domain. We solve the ideal induction equation (eq. [3]) without explicitly including any resistivity. Thus, only numerical diffusion is present and is very small in smooth regions, becoming significant only in regions with large gradients, e.g., at sites of intense current layers.

Figure 1 shows the setup of our simulation. The isothermal MHD equations are solved in a Cartesian domain (the box in Fig. 1) of size  $x = [-0.75L, 0.75L]$ ,  $y = [-0.5L, 0.5L]$ , and  $z = [0, 1.25L]$ , resolved by a  $240 \times 160 \times 200$  grid. At  $t = 0$ , the domain contains a potential arcade magnetic field

<sup>1</sup> The National Center for Atmospheric Research is sponsored by the National Science Foundation.

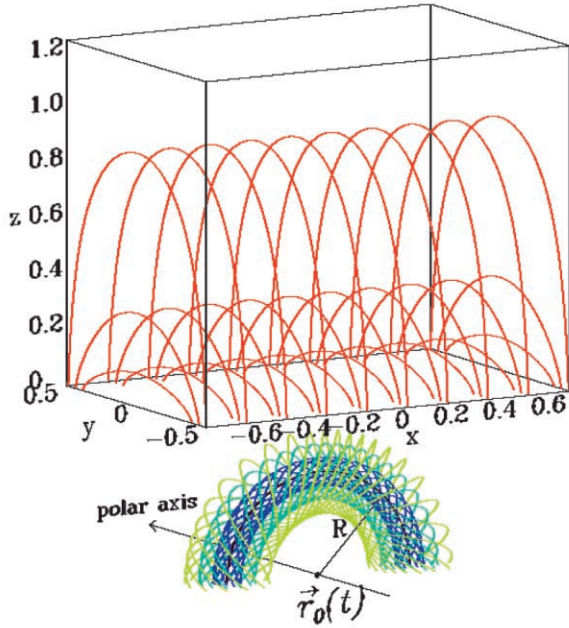


FIG. 1.—Setup of the numerical simulation (see text for description)

(the red field lines), whose vertical field at  $z = 0$  is confined into two bands:

$$B_z|_{z=0} = \begin{cases} B_0, & y < y_+, \\ B_0 \exp[-(y - y_+)^4/w^4], & y_+ < y < y_+ + 2w, \\ 0, & y_+ + 2w < y < y_- - 2w, \\ -B_0 \exp[-(y - y_-)^4/w^4], & y_- - 2w < y < y_-, \\ -B_0, & y_- < y, \end{cases} \quad (5)$$

where  $y_+ = -0.4L$ ,  $y_- = 0.4L$ , and  $w = 0.05L$ . At  $t = 0$ , the density  $\rho = \rho_0$  is assumed uniform in the box. The characteristic Alfvén speed in the box is  $v_A \equiv B_0/(4\pi\rho_0)^{1/2}$ . We use  $v_A$  and  $\tau_A \equiv L/v_A$  as the units for velocity and time. For  $t > 0$ , the computational domain is driven at the lower boundary by a  $\mathbf{v} \times \mathbf{B}$  electric field that corresponds to bodily lifting a twisted flux tube into the domain:

$$\mathbf{E}|_{z=0} = -\frac{1}{c}v_0\hat{z} \times \mathbf{B}_{\text{tube}}(x, y, z = 0, t), \quad (6)$$

where  $\mathbf{B}_{\text{tube}}$  is the magnetic field of a twisted flux tube. In a local spherical coordinate system with the origin at  $\mathbf{r}_0(t)$  (see Fig. 1),  $\mathbf{B}_{\text{tube}}$  is an axisymmetric toroidal flux tube given by  $\mathbf{B}_{\text{tube}} = \nabla \times [(r \sin \theta)^{-1}A(r, \theta)\hat{\phi}] + B_\phi(r, \theta)\hat{\phi}$ , with  $A = \frac{1}{2}qa^2B_i \times \exp(-\varpi^2/a^2)$ , and  $B_\phi = (r \sin \theta)^{-1}aB_i \exp(-\varpi^2/a^2)$ , where  $r$  is the radial distance from the origin  $\mathbf{r}_0(t)$ ,  $\theta$  is the polar angle from the polar axis (parallel to  $\hat{y}$ ),  $\hat{\phi}$  is the azimuthal direction,  $\varpi = (r^2 + R^2 - 2rR \sin \theta)^{1/2}$  is the distance to the tube axis (the black curve at  $r = R = 0.375L$  in Fig. 1), and  $B_i = 9B_0$ ,  $q = -1$ , and  $a = 0.1L$  are constants. Note that in Figure 1, only half of the toroidal flux tube is shown, and field lines on different toroidal flux surfaces are represented with different colors. Outside of the toroidal flux surface of  $\varpi = 3a$ ,  $\mathbf{B}_{\text{tube}}$  is truncated to zero. At the vicinity of the tube axis, field lines wind about the axis at a rate of  $q/a$  per unit length along the axis, and over the length of the semicircle shown in Figure 1, each field line

winds about the axis by about  $1.875 \times 2\pi$ . The flux tube  $\mathbf{B}_{\text{tube}}$  given above is not force-free. It is being transported into the computational domain (corona) via the time-dependent electric field at the lower boundary and is allowed to relax dynamically in the domain as governed by the isothermal MHD equations. In specifying  $\mathbf{E}|_{z=0}$  using equation (6), we assume that during  $0 < t < 54$ , the origin  $\mathbf{r}_0(t)$  is rising at a constant speed:  $\mathbf{r}_0(t) = (-0.675L + v_0t)\hat{z}$ , where  $v_0 = 0.0125v_A$ , and after  $t = 54$  when  $\mathbf{r}_0(t)$  has reached the lower boundary  $z = 0$ , we stop the rise and anchor the field lines by setting  $\mathbf{E}|_{z=0} = 0$ . We assume a uniform density  $\rho_0$  (same as the initial density in the domain) inside the emerging tube. Therefore, as the flux tube is being driven into the domain via  $\mathbf{E}|_{z=0}$ , there is also an inflow of mass flux  $\rho_0v_0$  through the lower boundary in the area where the emerging tube intersects the boundary. For the other boundaries of the computational domain, we assume perfect conducting walls for the side boundaries. At the top boundary, plasma and the magnetic field are allowed to flow through by simply extrapolating outward the values of velocity and density, and for the magnetic field, we assume that the field connects to a potential field above the domain. In our present simulation, we are mainly interested in the coronal magnetic field structure that can develop in response to the intrusion of a twisted flux tube that is transported into the domain via the artificial lower boundary conditions described above. Hence, the outstanding question concerning the complex dynamics of how a twisted flux tube can emerge as a whole from the high- $\beta$  interior through the photosphere boundary into the rarefied corona (Fan 2001; Magara & Longcope 2001, 2003) is not addressed.

### 3. RESULTS AND DISCUSSION

Panels 1a–4a and panels 1b–4b of Figure 2 show the three-dimensional evolution of the coronal magnetic field, driven at the lower boundary by the emergence of the twisted flux tube. Red field lines correspond to the anchored coronal arcade. For the emerging tube, field lines are color-coded based on the flux surfaces of the initial tube they belong to. The innermost black field lines are the ones near the tube axis. Figure 3 shows the evolution of the rise velocity  $v_r$  at the apex of the tube axis (*top panel*) and the angle of apex rotation due to the writhing motion (*bottom panel*). Note that the tube axis does not emerge from the lower boundary until  $t = 24$ . Since the velocity  $v_0 = 0.0125$  with which we transport the twisted flux tube through the lower boundary is very sub-Alfvénic, the earlier evolution of the emerging magnetic field in the corona is nearly quasi-static. As we can see in Figure 3, during the period from  $t = 25$  to about  $t = 45$ , the rise velocity  $v_r$  at the apex of the tube axis is roughly in pace with the transport velocity  $v_0$  at the lower boundary, and the axis of the emerging tube remains approximately in the  $(x, z)$ -plane without substantial writhing. However, after about  $t \sim 45$ , at which time the amount of field-line twist as measured by the angle ( $\Phi$ ) of field-line rotation about the axis between the footpoints of the emerged tube has reached about  $1.5 \times 2\pi$ , the tube undergoes a significant acceleration in both the rise and the writhing motion of the tube axis as a result of the onset of the kink instability. Hood & Priest (1981) conducted a stability analysis of a line-tied, uniformly twisted, force-free cylindrical flux tube and found that the tube becomes kink unstable when the amount of field-line twist between the line-tied ends exceeds a critical value of  $\Phi_{\text{cr}} = 1.25 \times 2\pi$ . In our present simulation, which is of a more complex three-dimensional arched twisted flux tube, the field-line twist ( $\Phi \sim 1.5 \times 2\pi$ ) for which the emerging tube begins

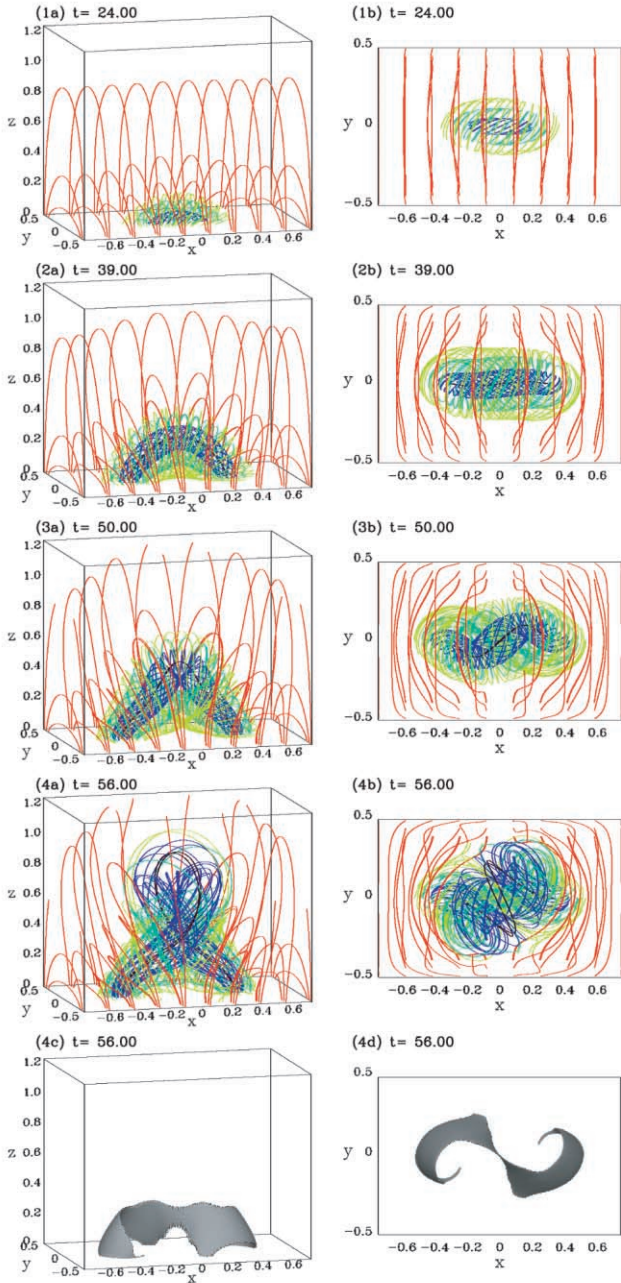


FIG. 2.—Snapshots of the three-dimensional evolution of the coronal magnetic field as viewed from the side (panels 1a–4a) and from the top (panels 1b–4b) and the three-dimensional isosurface (level set at  $20B_0/L$ ) of the electric current density  $j$  in the corona as viewed from the side (panel 4c) and from the top (panel 4d) corresponding to the same time as snapshots 4a and 4b.

to develop substantial writhing is somewhat larger than the critical value obtained in Hood & Priest (1981). We find with a separate numerical experiment that if we stopped the emergence (set  $v_0$  to zero in eq. [6]) at  $t = 39$  when the amount of field-line twist between the footpoints reaches the critical value ( $\Phi = 1.25 \times 2\pi$ ) of Hood & Priest (1981), the emerged tube settles into an equilibrium structure that is very close to that shown in panels 2a and 2b of Figure 2 without developing significant writhing (the tilt angle at the apex is about  $8^\circ$ ). In our present simulation shown in Figures 2 and 3, we continue driving the flux tube emergence until  $t = 54$  when  $\Phi$  reaches  $1.875 \times 2\pi$ . The flux tube develops substantial writhing with

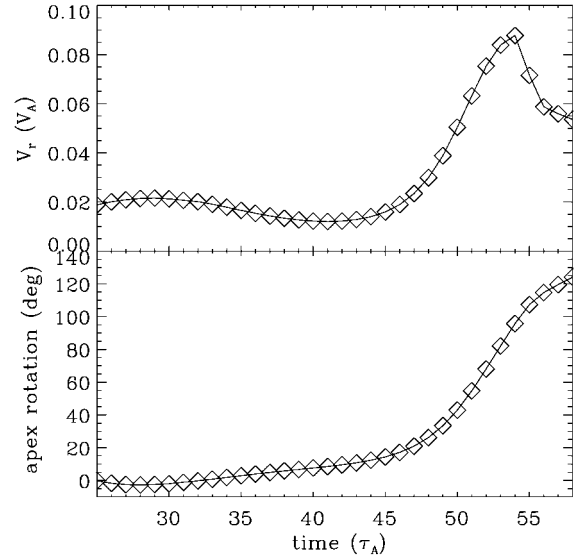


FIG. 3.—Evolution of the rise velocity  $v_r$  at the apex of the tube axis (top panel) and the angle of apex rotation due to the writhing motion (bottom panel).

an anticlockwise rotation at the apex of the tube axis reaching about  $120^\circ$  at  $t = 56$  (see Fig. 3 and panels 4a and 4b of Fig. 2). As a result of stopping the emergence at  $t = 54$ , the rise velocity and the writhing motion at the apex show a deceleration (see Fig. 3); however, we do not find that the tube reaches a new kinked equilibrium before it moves out of our computational domain.

An important result that we found from our present simulation is the structure of the electric current concentration as the emerging tube becomes highly kinked and its possible connection to the X-ray sigmoid morphology. The conservation of helicity requires that the writhing of the flux tube axis as a result of the kink instability be of the same sense as the twist of the tube (Linton et al. 1999; Fan et al. 1999). Therefore, for our left-hand-twisted emerging tube, the writhing is also left-handed, resulting in a forward-S shape for the upward-protruding tube axis as viewed from the top (see the black field lines in panels 3b and 4b of Fig. 2). Active regions at the photosphere show a preferentially left-handed twist in the northern hemisphere, the same sense as our emerging tube. However, the coronal X-ray sigmoids seen in the northern hemisphere have preferentially inverse-S morphology, opposite to the forward-S shape of our kinked tube axis. In fact, we can easily identify both forward- and inverse-S-shaped field lines in the emerged tube (see also Magara & Longcope 2003 and Abett & Fisher 2003). Note that a field line with a left-handed writhe can appear as either a forward-S or an inverse-S, when viewed from the top, depending on whether it is upward-protruding or dipped. In Magara & Longcope (2003), the axial field line of their left-hand-twisted emerging tube shows a slight inverse-S shape (see their Figs. 2d and 2e) because it dips downward as a result of the plasma weight (which also inhibits the kink instability). In our low- $\beta$  coronal simulation (in which gravity is ignored), the axis protrudes upward and shows a forward-S shape. Given the presence of S-shaped field lines of both directions in the emerged tube, field-line geometry itself clearly cannot explain X-ray sigmoids. Since X-ray sigmoids are most likely sites of enhanced heating due to the formation of strong electric current layers (e.g., Titov & Demoulin 1999; Low & Berger 2003), we examine the three-dimensional current distribution. During the initial

quasi-static evolution before the onset of the kink instability, we find that the dominant current in the corona is simply the volume current that flows along the twisted emerging tube. Due to the high electric conductivity in the corona, such volume currents are not expected to be dissipated: intense thin current layers are necessary for magnetic reconnection and significant heating (Parker 1994; Longcope & Strauss 1994). As the twisted flux tube develops substantial writhing as a result of the kink instability, we find that a new curved layer of a highly concentrated current forms and becomes the dominant feature in the current distribution in the corona. Panels 4c and 4d of Figure 2 show the three-dimensional isosurface of the electric current density  $j = |\nabla \times \mathbf{B}|$  in the corona corresponding to the field shown in panels 4a and 4b at  $t = 56$ . The level for the  $j$  isosurface is set to a value of  $20B_0L^{-1}$ . As viewed from the top (see panel 4d of Fig. 2), the curved layer of current concentration shows an inverse-S shape, consistent with the morphology of X-ray sigmoids in the northern hemisphere. Figure 4 shows (at  $t = 56$ ) a horizontal slice at height  $z = 0.25$  of the vertical magnetic field  $B_z$  overlaid with arrows of the horizontal magnetic field (Fig. 4a) and also a horizontal slice at the same height of the current density  $j$  (Fig. 4b). We see that the inverse-S-shaped current layer, which is the strongest current concentration in the domain, is aligned with the neutral line of  $B_z$ , where oppositely directed  $B_z$  is being forced together, producing a sharp gradient. In Figure 4a, the upper left and lower right portions of this inverse-S-shaped neutral line correspond to the boundaries between the opposite  $B_z$  of the flux tube and the ambient arcade, and the middle portion of the neutral line corresponds to the boundary between the opposite  $B_z$  of the two legs of the tube.

The question remains whether the inverse-S-shaped current layer will indeed brighten up as an X-ray sigmoid. This requires a quantitative determination of the current density and heating rate that cannot be addressed within our present simulations. In our simulation, the thin current layer is subject to broadening by the numerical diffusion to a few grid zones to ensure nu-

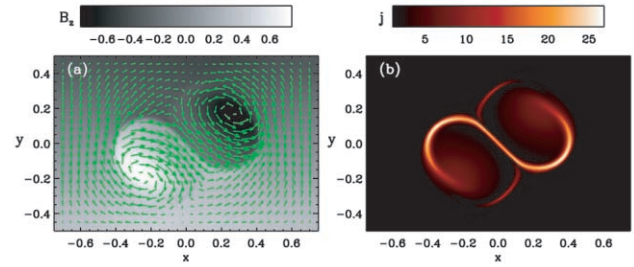


FIG. 4.—(a) Horizontal slice at height  $z = 0.25$  of the vertical magnetic field  $B_z$  overlaid with arrows of the horizontal magnetic field; (b) horizontal slice at the same height of the current density  $j$ , at time  $t = 56$ .

merical stability. Thus, due to the limited grid resolution of our three-dimensional simulation, the current layer is most likely underresolved, and its current density grossly undervalued. However, our simulation does provide information on the location and morphology of the strong current concentrations that will form as a result of forcing by the kink motion of the tube. Titov & Demoulin (1999) studied analytically the quasi-static emergence of a twisted flux tube embedded in a potential bipolar field and predicted the formation of a strong current layer at the separatrix surface between winding and nonwinding fields for the onset of the kink instability, which appears to be consistent with the location of the inverse-S-shaped current layer found here. A comparison of our dynamic simulations with a detailed analysis of the separatrix surface at various states of emergence (similar to that carried out in Titov & Demoulin 1999 and Gibson et al. 2002) will be the subject of a subsequent paper.

We thank B. C. Low and Keith MacGregor for helpful discussions. This work is supported in part by AFOSR grant F49620-02-0191.

#### REFERENCES

- Abbett, W. P., & Fisher, G. H. 2003, *ApJ*, 582, 475  
 Canfield, R. C., Hudson, H. S., & McKenzie, D. E. 1999, *Geophys. Res. Lett.*, 26, 627  
 Fan, Y. 2001, *ApJ*, 554, L111  
 Fan, Y., Zweibel, E. G., Linton, M. G., & Fisher, G. H. 1999, *ApJ*, 521, 460  
 Gibson, S. E., Low, B. C., Leka, K. D., Fan, Y., & Fletcher L. 2002, in *SOLMAG 2002: Proc. Magnetic Coupling of the Solar Atmosphere Euroconf. and IAU Colloq. 188*, ed. H. Sawaya-Lacoste (ESA SP-505; Noordwijk: ESA), 265  
 Hood, A. W., & Priest, E. R. 1981, *Geophys. Astrophys. Fluid Dyn.*, 17, 297  
 Linton, M. G., Fisher, G. H., Dahlburg, R. B., & Fan, Y. 1999, *ApJ*, 522, 1190  
 Longcope, D. W., & Strauss, H. R. 1994, *ApJ*, 437, 851  
 Low, B. C., & Berger, M. 2003, *ApJ*, 589, 644  
 Magara, T., & Longcope, D. W. 2001, *ApJ*, 559, L55  
 ———. 2003, *ApJ*, 586, 630  
 Parker, E. N. 1994, *Spontaneous Current Sheets in Magnetic Fields* (New York: Oxford Univ. Press)  
 Pevtsov, A. A., Canfield, R. C., & Latushko, S. M. 2001, *ApJ*, 549, L261  
 Rust, D. M., & Kumar, A. 1996, *ApJ*, 464, L199  
 Titov, V. S., & Demoulin, P. 1999, *A&A*, 351, 707